

Complex frequencies and field distributions of localized surface plasmon modes in graphene-coated subwavelength wires

MÁXIMO A. RISO¹, MAURO CUEVAS², AND RICARDO A. DEPINE^{1,*}

¹Grupo de Electromagnetismo Aplicado, Departamento de Física, FCEN, Universidad de Buenos Aires and IFIBA, Consejo Nacional de Investigaciones Científicas y Técnicas (CONICET), Ciudad Universitaria, Pabellón I, C1428EHA, Buenos Aires, Argentina

²Facultad de Ingeniería y Tecnología Informática, Universidad de Belgrano, Villanueva 1324, C1426BMJ, Buenos Aires, Argentina and Consejo Nacional de Investigaciones Científicas y Técnicas (CONICET)

*Corresponding author: rdep@df.uba.ar

Compiled October 16, 2015

In this work we study the modal characteristics of localized surface plasmons in graphene-coated, circular cross-section wires. Localized surface plasmons are represented in terms of cylindrical multipole partial waves characterized by discrete, complex frequencies that depend on the size of the wire and that can be dynamically tuned via a gate voltage. We consider both intrinsically nonplasmonic wires and intrinsically plasmonic wires. In the first case the localized surface plasmons are introduced by the graphene coating, whereas in the second case the localized eigenmodes of the graphene coating are expected to hybridize those already existing in the bare wire. We show that the approach presented here, valid for particle sizes where the retardation effects can be significant, agree well with analytical expressions obtained in the limit when the particle size is very small compared to the wavelength of the eigenmode. © 2015 Optical Society of America

OCIS codes: 160.0160 Materials; (160.4760) Optical properties; (250.5403) Plasmonics

<http://dx.doi.org/10.1364/ao.XX.XXXXXX>

1. INTRODUCTION

The coherent coupling of photons to free electron oscillations at the interface between a conductor and a dielectric results in the formation of surface electromagnetic modes known as surface plasmons. In bounded geometries these modes, called localized surface plasmons (LSPs), are characterized by discrete, complex frequencies that depend on the size and shape of the object to which they are confined. Excitation of LSPs results in an enhancement of the local electromagnetic field as well as in the appearance of intense absorption bands. Moreover, the efficiency of light scattering from plasmonic particles is also enhanced under resonant excitation of LSPs, a fact that plays key roles in many areas that requires control, manipulation and trapping of light [1]. For example, the high surface sensitivity of LSPs from single nanoparticles can be used to monitor single-molecule chemical events [2] and the enhancement of the local electromagnetic field can be used to largely enhance single-molecule fluorescence [3].

Apart from noble metals—the plasmonic materials most frequently used for visible and near IR applications—recent advances have created other plasmonic materials that allow dy-

namic manipulation of carrier densities, such as doped semiconductors nanocrystals [4]. In the search for plasmonic materials with lower losses and greater confinement of the electromagnetic energy [5], the advent of graphene [6] has led to many promising new opportunities for future plasmonic applications.

Graphene is a 2-D sheet of carbon atoms arranged in a honeycomb lattice [6] that supports long-lived, electrically tunable surface plasmons [7] and potentially enables new optoelectronic applications in the terahertz frequency range [8]. The propagation characteristics of graphene plasmonic waveguides have been investigated in different planar structures, such as infinite sheets [9], ribbons [10, 11] or grooves [12]. Recent experiments showing that, thanks to the van der Waals force, particles with various shapes and sizes can be wrapped up with graphene sheets [13–20], have been the motivation for two kind of theoretical studies on plasmonic graphene layers wrapped around dielectric core objects, one devoted to the *propagation* of graphene plasmons along the axis of graphene-coated nanowire waveguides [21–23] and the other to the *excitation* of LSPs with an electromagnetic plane wave in spherical [24, 25] and cylindrical particles [26, 27]. This paper is devoted to the study of LSPs

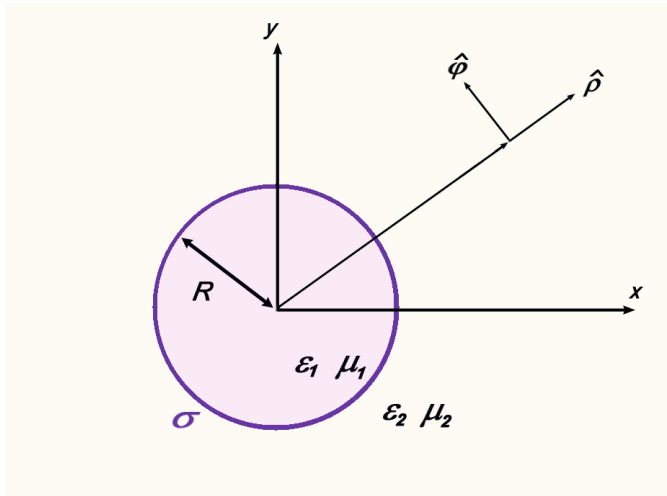


Fig. 1. Graphene-coated cylinder with circular cross-section. The graphene layer is characterized by a frequency dependent surface conductivity σ .

supported by graphene coated circular cross-section wires. Our main objective is to obtain the full characteristics (complex frequencies and field distributions) of these LSPs, but instead of using a scattering approach with an incident electromagnetic wave to produce the excitations (the procedure used in Refs. [24] and [25] for spheres and in Refs. [26] and [27] for cylinders), here we formulate the LSP problem *in absence of incident fields*, a formulation which is better suited for the determination of both plasmon resonance frequencies and plasmon decay rates (or damping times). This is so because in the formulation with incident fields (inhomogeneous problem), plasmon resonance frequencies and plasmon decay rates can be determined only indirectly, through the observation of positions of maxima or widths of resonances in scattering cross-section spectra. On the other hand, in the formulation without incident fields presented here (homogeneous problem), plasmon frequencies and plasmon decay rates appear as intrinsic eigenproperties obtained in a direct manner from the real and imaginary parts of complex modal frequencies. The dependence of these complex frequencies on the size of the wire, the conductivity of the graphene coating and the electromagnetic constitutive parameters of the core is essential for controlling the spectral properties of plasmonic particles for technological or diagnostic applications. The real part of the complex frequencies gives the position of maxima in scattering spectra, whereas the imaginary part, an important parameter for transient and nonlinear phenomena [28], provides useful information about the full characteristics of surface plasmons, such as radiation and ohmic losses, and is closely related to the spectral width of the resonant coupling and to the lifetime of surface plasmons. This fact is important for most applications that requires to control the spectral response of the plasmonic particle, such as the ability of plasmonic nanoantennas in receiving and transmitting radiation [29].

The plan of this paper is as follows. In section 2 we describe LSPs in graphene-coated, circular cross-section wires in terms of cylindrical multipole partial waves characterized by complex frequencies and we give the main steps for the derivation of the dispersion equation for the eigenfrequencies and the calculation of their corresponding field distributions. The method is not limited to any particular range of radius/wavelength ratios

and applies for large particles, where retardation effects may be significant. In section 3 we offer alternative simpler results obtained using the small-argument asymptotic expansions for the Bessel functions and valid in the quasistatic regime in which the radius/wavelength ratio is small. In this regime we provide analytical expressions for the plasmon resonance frequency and the plasmon decay rate for two different kind of wire cores: nondispersive dielectric (nonplasmonic) cores and Drude dispersive (plasmonic) cores. The characteristics of LSPs, including dispersion relation, mode patterns and their dependence on wire radius, substrate permittivity and chemical potential of graphene are illustrated in Section 4. In the last part of this section we correlate the homogeneous problem results obtained with this approach with those obtained through the observation of positions of maxima and widths of resonances in scattering cross-section spectra. Finally, in Section 5 we summarize and discuss the results obtained. The Gaussian system of units is used and an $\exp(-i\omega t)$ time-dependence is implicit throughout the paper, with ω the angular frequency, t the time, and $i = \sqrt{-1}$.

2. HOMOGENEOUS PROBLEM

We consider a graphene-coated cylinder with circular cross-section (radius R) centered at $x=0, y=0$ (see Figure 1). The wire substrate is characterized by the electric permittivity ϵ_1 and the magnetic permeability μ_1 and may be dielectric or conducting. The wire is embedded in a transparent medium with electric permittivity ϵ_2 and magnetic permeability μ_2 . The graphene layer is treated as an infinitesimally thin, local and isotropic two-sided layer with surface conductivity σ given by the Kubo formula [30, 31]

$$\sigma(\omega) = \frac{i e^2 \mu_c}{\pi \hbar^2 (\omega + i\gamma_c)} + \frac{e^2}{4\hbar} \left\{ \Theta(\hbar\omega - 2\mu_c) - \frac{i}{\pi} \ln \left| \frac{\hbar\omega + 2\mu_c}{\hbar\omega - 2\mu_c} \right| \right\}, \quad (1)$$

where $\Theta(x)$ is the Heaviside function, e is the electron charge and \hbar is the reduced Planck constant. Apart from the angular frequency ω , the value of σ depends on the chemical potential μ_c (controlled with the help of a gate voltage), the ambient temperature T and the carriers scattering rate γ_c . The first term in Eq. (1) – the term which dominates at low temperatures $\mu_c \gg k_B T$ – is a generalization of the Drude model for the case of arbitrary band structure and represents contributions from intraband transitions, whereas the second term in Eq. (1) – the term which dominates for large doping – represents contributions from interband transitions.

In order to derive complex frequencies and field distributions of LSP modes in terms of the radius R of the wire, the constitutive parameters of substrate and ambient media and the parameters of the graphene surface conductivity, we use an accurate electrodynamic formalism which closely follows the usual separation of variables approach. The problem is formulated in absence of incident fields. For surface plasmons localized around the cylinder section the modal problem can be handled in a scalar way since in this case the most general electromagnetic field can be described as a linear combination of solutions obtained in two fundamental scalar problems: electric field parallel to the main section of the cylindrical surface (p polarization or $E_z=0$ modes) and magnetic field parallel to the main section of the cylindrical surface (s polarization or $H_z=0$ modes). Moreover, LSPs are not supported in s polarization since in this case the electric field in the graphene coating can only induce electric currents directed along the wire axis, and not along the azimuthal

direction $\hat{\varphi}$ as is required for LSPs to exist in the graphene circular cylinder. The magnetic field $\vec{H}_n(\rho, \varphi, t)$ corresponding to the n -th LSP mode is written as

$$\vec{H}_n(\rho, \varphi, t) = F_n(\rho, \varphi) \exp(-i\omega_n t) \hat{z}, \quad (2)$$

where ω_n is the modal frequency. Taking into account that, due to radiation losses and relaxation processes plasmon oscillations are always damped, the modal frequencies must be represented by complex numbers. The spatial part of the magnetic field $F(\rho, \varphi)$ is expanded as series of cylindrical harmonics in the internal and external regions.

$$F_n(\rho, \varphi) = \begin{cases} c_n \mathcal{J}_n(k_1 \rho) \exp in\varphi, & \rho < R, \\ a_n \mathcal{H}_n^{(1)}(k_2 \rho) \exp in\varphi, & \rho > R, \end{cases} \quad (3)$$

where a_n and c_n are complex coefficients, $n = 1, 2, \dots, \infty$, $k_j = \frac{\omega}{c} \sqrt{\epsilon_j \mu_j}$ ($j = 1, 2$), c is the speed of light in vacuum, and \mathcal{J}_n and $\mathcal{H}_n^{(1)}$ are the n -th Bessel and Hankel functions of the first kind respectively. The boundary conditions for the graphene-coated cylinder at $\rho = R$ are

$$\frac{1}{\epsilon_2} \frac{\partial F_n}{\partial \rho} \Big|_{R^+} = \frac{1}{\epsilon_1} \frac{\partial F_n}{\partial \rho} \Big|_{R^-}, \quad F_n \Big|_{R^+} - F_n \Big|_{R^-} = \frac{4i\pi}{\omega \epsilon_1} \sigma \frac{\partial F_n}{\partial \rho} \Big|_{R^+}. \quad (4)$$

Introducing expressions (3) into the boundary conditions, a set of two homogeneous equations is obtained

$$\frac{k_2}{\epsilon_2} a_n \mathcal{H}_n^{(1)'}(k_2 R) = \frac{k_1}{\epsilon_1} c_n \mathcal{J}_n'(k_1 R), \quad (5)$$

$$a_n \mathcal{H}_n^{(1)}(k_2 R) - c_n \mathcal{J}_n(k_1 R) = \frac{4\pi}{c} \sigma i \frac{ck_1}{\omega \epsilon_1} c_n \mathcal{J}_n'(k_1 R), \quad (6)$$

where the prime denotes the first derivative with respect to the argument of the function. In order to have a nontrivial solution, the following condition is required

$$\mu_2 h_n - \mu_1 j_n + \frac{4\pi}{c} \sigma \frac{\omega}{c} i R \mu_1 \mu_2 j_n h_n = 0, \quad (7)$$

where

$$j_n = \frac{\mathcal{J}_n'(k_1 R)}{k_1 R \mathcal{J}_n(k_1 R)} \quad h_n = \frac{\mathcal{H}_n^{(1)'}(k_2 R)}{k_2 R \mathcal{H}_n^{(1)}(k_2 R)} \quad (8)$$

Equation (7) is the dispersion relation for the plasmonic eigenmodes of the graphene-coated cylinder and it gives the complex frequency ω_n for the LSP represented by the cylindrical multipole partial wave given by Eq. (2). Once the eigenvalues and their corresponding complex amplitudes a_n, c_n have been found, the spatial part of the electromagnetic field for the n th mode is given by

$$\vec{H}_n = \begin{cases} \mathcal{J}_n(k_1 \rho) \exp in\varphi \hat{z}, & \rho < R, \\ \frac{k_1 \epsilon_2}{k_2 \epsilon_1} \frac{\mathcal{J}_n'(k_1 R)}{\mathcal{H}_n^{(1)'}(k_2 R)} \mathcal{H}_n^{(1)}(k_2 \rho) \exp in\varphi \hat{z}, & \rho > R, \end{cases} \quad (9)$$

$$\vec{E}_n = \begin{cases} \frac{ick_1}{\omega \epsilon_1} \left(in \frac{\mathcal{J}_n(k_1 \rho)}{k_1 \rho} \hat{\rho} - \mathcal{J}_n'(k_1 \rho) \hat{\varphi} \right) \exp in\varphi, & \rho < R, \\ \frac{ick_1}{\omega \epsilon_1} \frac{\mathcal{J}_n'(k_1 R)}{\mathcal{H}_n^{(1)'}(k_2 R)} \left(in \frac{\mathcal{H}_n^{(1)}(k_2 \rho)}{k_2 \rho} \hat{\rho} - \mathcal{H}_n^{(1)'}(k_2 \rho) \hat{\varphi} \right) \exp in\varphi, & \rho > R. \end{cases} \quad (10)$$

3. QUASISTATIC APPROXIMATION

A. Non retarded dispersion relation

Equation (7) gives the fully-retarded dispersion relation. When the size of the wire is small compared to the eigenmode wavelength ($R \ll \lambda_n = \text{Re} 2\pi c / \omega_n$), we use the quasistatic approximation. Using the small argument asymptotic expansions for Bessel and Hankel functions [32], it follows that the functions in Eq. (8) can be approximated by $j_n(x) \rightarrow n/x^2$ and $h_n(x) \rightarrow -n/x^2$ and therefore Eq. (7) adopts the form

$$\epsilon_1 + \epsilon_2 = -\frac{4\pi}{c} \sigma \frac{c}{\omega} \frac{i}{R} n. \quad (11)$$

This is the resonance condition for a collective electron oscillation in a graphene-coated thin wire that is excited by an electric field polarized perpendicular to the wire axis. When $\sigma = 0$, it reduces to the plasmon resonance condition of a thin metallic wire [33]. From Eq. (11) it is evident that for graphene coatings with $\text{Im} \sigma > 0$, LSPs may exist in a dielectric wire even when $\epsilon_1 \epsilon_2 > 0$, although in the absence of a coating the existence of LSPs usually requires a metallic medium, *i.e.*, $\epsilon_1 \epsilon_2 < 0$.

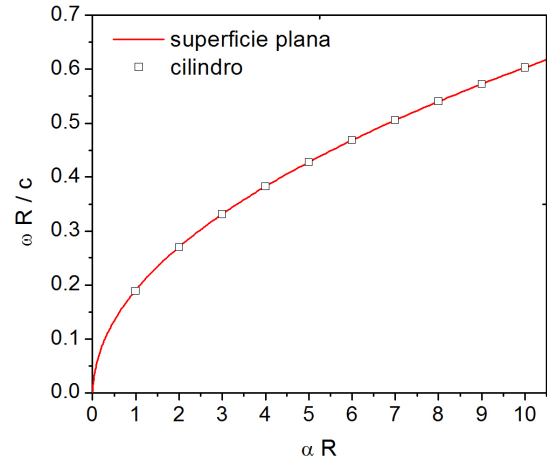



Fig. 2. Comparison between the exact real part of the modal frequency values computed from Eq. (7) and the curve $\text{Re} \omega(k_{SP})$ corresponding to a perfectly flat graphene sheet (continuous lines) with $\gamma_c = 0.1 \text{ meV}$, $\epsilon_1 = 2.13$, $\mu_1 = \mu_2 = \epsilon_2 = 1$. a) $R = xx \mu\text{m}$, b) $R = yy \mu\text{m}$, 

Taking into account that in the nonretarded regime the wavenumber k_{SP} for propagating surface plasmons in perfectly flat, infinite graphene sheets can be approximated by [9]

$$k_{SP} = \frac{\omega}{c} i \frac{\epsilon_1 + \epsilon_2}{4\pi\sigma/c}, \quad (12)$$

we observe that the dispersion Eq. (11) for localized surface plasmons in graphene-coated cylinders can be rewritten in the form

$$k_{SP} 2\pi R = 2\pi n, \quad (13)$$

which can be interpreted in the way that the n -th LSP mode of a graphene-coated cylinder accommodates along the cylinder perimeter exactly n oscillation periods of the propagating surface plasmon corresponding to the flat graphene sheet. A rather similar result has been obtained in graphene-coated nanospheres

in an uniform background, but for LSPs with high values of the orbital angular momentum order [24]. For the cylinder case considered here the result (13) is valid for all multipolar orders, although it is restricted to the limits of the quasistatic approximation and the higher the multipole modal frequency ω_n the better this approximation holds, since the effective wavelength of higher multipoles become shorter and the LSP modes perceive the circular graphene sheet as increasingly flat. To test the prediction from Eq. (13) we compare in Figure 2 the real part of the exact modal frequency computed from the fully retarded dispersion relation Eq. (7) against the curve ω versus k_{SP} corresponding to the perfectly flat graphene sheet (continuous lines). **Como ven, propongo poner acá las curvas de la discretización del plasmón del plano, en vez de las que estaban. De ser así, ponemos dos valores de R, uno grande y uno chico? Tiene sentido comparar también las partes imaginarias?** We observe that in the case $R = xx$ the agreement is excellent for all the multipolar modal frequencies ω_n , whereas in the case $R = yy$ the approximation (13) ceases to be valid for the lowest modal frequencies.

B. Analytical expressions for ω_n

Although useful to provide an enlightening connection between localized and nonlocalized graphene surface plasmons, Eq. (11) requires numerical schemes to find its complex roots ω_n . For large doping ($\mu_c \gg k_B T$) and relatively low frequencies ($\hbar\omega_n < \mu_c$) the intraband contribution to the surface conductivity (the first term in Eq. (1), the Drude term) plays the leading role. In this case, Eq. (11) takes a simpler form

$$\varepsilon_1 + \varepsilon_2 = \frac{4e^2 \mu_c n}{\hbar^2 R (\omega + i\gamma_c) \omega}, \quad (14)$$

which allows us to obtain analytic expressions for the plasmon eigenfrequencies in the particular cases of non-dispersive and dispersive interiors.

Let us first consider a non-dispersive dielectric interior such as a polymer. In this case Eq. (14) can be rewritten as

$$(\varepsilon_1 + \varepsilon_2) \omega^2 + i(\varepsilon_1 + \varepsilon_2) \gamma_c \omega - \omega_{0n}^2 = 0, \quad (15)$$

where $\omega_{0n}^2 = 4e^2 \mu_c n / (\hbar^2 R)$ is the effective plasma-frequency of the graphene coating for the n -th mode. Solving this quadratic equation, we obtain the following analytical expression for the eigenmode frequencies

$$\omega_n = \sqrt{\frac{\omega_{0n}^2}{\varepsilon_1 + \varepsilon_2} - \left(\frac{\gamma_c}{2}\right)^2} - i \frac{\gamma_c}{2} \approx \frac{\omega_{0n}}{\sqrt{\varepsilon_1 + \varepsilon_2}} - i \frac{\gamma_c}{2}, \quad (16)$$

the second equality holding when $\gamma_c \ll \omega_0$.

In the second case, we consider that the substrate of the graphene-coated wire is a dispersive, metallic-like material, with $\varepsilon_1(\omega)$ represented by the Drude model

$$\varepsilon_1(\omega) = \varepsilon_\infty - \frac{\omega_p^2}{\omega^2 + i\gamma_m \omega}, \quad (17)$$

where ε_∞ is the high-frequency dielectric permittivity, γ_m is the damping constant and ω_p is the plasma frequency. Equation (17) is used to describe strongly doped semiconductors much larger in extent than the Fermi wavelength [4]. Replacing Eq. (17) into Eq. (14) we obtain

$$\varepsilon_\infty + \varepsilon_2 = \frac{\omega_p^2}{\omega^2 + i\gamma_m \omega} + \frac{\omega_{0n}^2}{\omega^2 + i\gamma_c \omega}, \quad (18)$$

which can be rewritten as

$$\omega^2(\varepsilon_\infty + \varepsilon_2) = \frac{\omega_p^2}{1 + ix} + \frac{\omega_{0n}^2}{1 + iy}, \quad (19)$$

with $x = \frac{\gamma_m}{\omega}$ and $y = \frac{\gamma_c}{\omega}$. After expanding the right hand side of Eq. (19) in powers of x and y and retaining only the first order terms, Eq. (19) can be rewritten as

$$(\varepsilon_\infty + \varepsilon_2) \omega^3 - (\omega_p^2 + \omega_{0n}^2) \omega + (\omega_p^2 \gamma_m + \omega_{0n}^2 \gamma_c) i = 0. \quad (20)$$

Separating the frequency into its real and imaginary parts, $\omega = \omega_R - i\omega_I$, $\omega_R > 0$, $\omega_I > 0$ we get

$$E[\omega_R^3 - 3\omega_R \omega_I^2] + iE[\omega_I^3 - 3\omega_R^2 \omega_I] - \Omega^2 \omega_R + \Omega^2 i \omega_I + \Gamma i = 0,$$

where we have neglected cubic and quartic terms in ω_I and $E = \varepsilon_\infty + \varepsilon_2$, $\Omega^2 = \omega_p^2 + \omega_{0n}^2$, $\Gamma = \omega_p^2 \gamma_m + \omega_{0n}^2 \gamma_c$. Finally, the following analytical expressions are obtained for the real and imaginary parts of the eigenmode frequencies

$$\omega_{Rn} = \sqrt{\frac{\omega_p^2 + \omega_{0n}^2}{\varepsilon_\infty + \varepsilon_2}} \quad \omega_{In} = \frac{\omega_p^2 \gamma_m + \omega_{0n}^2 \gamma_c}{2(\omega_p^2 + \omega_{0n}^2)}. \quad (21)$$

4. RESULTS

We illustrate the characteristics of LSPs in two different kind of graphene coated wires, one with nondispersive dielectric, intrinsically nonplasmonic cores and the other with Drude dispersive, intrinsically plasmonic cores. In all the examples the core is non magnetic ($\mu_1 = 1$) and is embedded in vacuum ($\varepsilon_2 = \mu_2 = 1$).

A. Nondispersive dielectric wires

For nondispersive dielectric cores and for the case considered in Figure 2a we have already seen that the values $\text{Re } \omega_n$ computed with the fully-retarded (FR) dispersion equation Eq. (7) agree well with those obtained with the quasistatic (QS) approximation Eq. (11). In Table 1 we compare FR ω_n values with those obtained using the analytical approximation (AA), that is, Eq. (16) for $R = 0.5 \mu\text{m}$, $\mu_c = 0.5 \text{ eV}$, $\gamma_c = 0.1 \text{ meV}$, $\varepsilon_1 = 2.13$ (corresponding to Polymethylpentene) and $1 \leq n \leq 10$. Since the radius of the wire is small compared with the eigenmode wavelengths, good agreement is obtained between the complex FR and AA ω_n values, even when the AA assigns $\text{Im } \omega_n = -\gamma_c/2$ to all multipolar plasmon modes, i.e., $\text{Im } \omega_n/c = -0.5\gamma_c/c \approx -0.00025 \mu\text{m}^{-1}$. Maps of the internal modal magnetic field $\vec{H}_n(\rho, \varphi)$ calculated

n	FR	AA
1	0.2159 - i0.88 10 ⁻³	0.xxxx - i0.25 10 ⁻³
2	0.3066 - i0.26 10 ⁻³	0.xxxx - i0.25 10 ⁻³
3	0.3759 - i0.25 10 ⁻³	0.xxxx - i0.25 10 ⁻³
4	0.4342 - i0.25 10 ⁻³	0.xxxx - i0.25 10 ⁻³

Table 1. FR and AA ω_n/c values in μm^{-1} for the first four modes, $R = 0.5 \mu\text{m}$, $\gamma_c = 0.1 \text{ meV}$, $\varepsilon_1 = 2.13$ and $\mu_1 = \mu_2 = \varepsilon_2 = 1$.

with the first equation in (9) at a fixed time are shown in Figure 3a for the first four modes shown in Table 1. We observe that the field distribution follows typical dipolar, quadrupolar, hexapolar and octopolar patterns. The angular dependence of the modes,

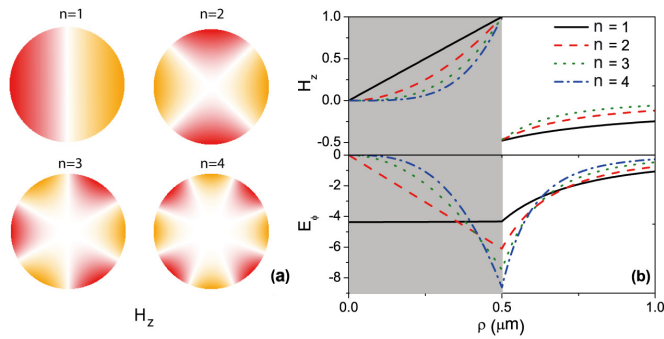


Fig. 3. (a) Map of $H_{nz}(\rho, \varphi)$ at a fixed time for the first four modes of the wire considered in Table 1. Red, positive values, orange, negative values. (b) Radial dependence of H_{nz} (top) and $E_{n\varphi}$ (bottom) near $\rho = R$ at ω_n/c . The parameters are $\gamma_c = 0.1$ meV, $R = 0.5 \mu\text{m}$, $\varepsilon_1 = 2.13$ and $\mu_1 = \mu_2 = \varepsilon_2 = 1$. **Propongo sacar c y d, para que se luzcan las figuras de los campos que son muy lindas. Y no cansar con el tema dispersión. Por ahora comenté esta parte en el texto, pero se puede volver a incluir.**

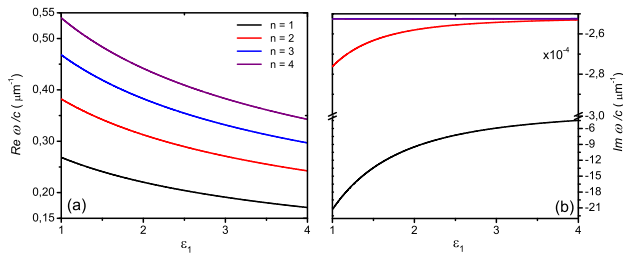


Fig. 4. FR values of $\text{Re } \omega_n$ (a) and $\text{Im } \omega_n$ (b) for $1 \leq n \leq 4$ as functions of the permittivity ε_1 , for $\varepsilon_2 = 1$, $R = 0.5 \mu\text{m}$, $\mu_c = 0.5\text{eV}$, $\gamma_c = 0.1$ meV and $\mu_1 = \mu_2 = 1$.

given by $\exp(in\varphi)$, is the same for all the field components. Therefore, in order to visualize field distributions we evaluated the radial behavior described by Eq. (9). Figure 3b shows these ρ -dependent amplitudes for the field components $\text{Re } H_{nz}(\rho)$ and $\text{Im } E_{n\varphi}(\rho)$, with $n = 1, 2, 3$ and 4 . We have chosen the normalization $|H_z| = 1$ at the boundary of the wire ($\rho = R$). Since the values ω_n are almost real numbers, ($|\text{Re } \omega_n / \text{Re } \omega_n| \approx 10^{-3}$, $1 \leq n \leq 4$), the arguments of the Bessel and Hankel functions in (9) and (10) are almost real numbers. As a consequence, the ρ -dependent part of $H_{nz}(\rho)$ takes almost purely real values whereas the ρ -dependent part of $E_{n\varphi}$ takes almost purely imaginary values. Due to the presence of a surface current density $j_\varphi = \frac{4\pi}{c} \sigma E_\varphi$ induced on the graphene sheet and according to the boundary conditions in Eq. (4), a discontinuity at $\rho = R$ is observed in Figure 3b for $H_{nz}(\rho)$, whereas $E_{n\varphi}(\rho)$ is continuous at $\rho = R$. Strong field confinements are also observed near $\rho = R$, with higher confinements for the higher modes.

In order to evaluate the dependence of the complex eigenfrequencies on the contrast between external and internal constitutive parameters, in Figures 4a and 4b we show the FR values of $\text{Re } \omega_n$ and $\text{Im } \omega_n$, $1 \leq n \leq 4$, as functions of the permittivity of the internal medium ε_1 , the other parameters as in Figure ???. We observe that $\text{Re } \omega_n/c$ is maximum for the case of a graphene cylinder in a uniform background ($\varepsilon_1 = \varepsilon_2 = 1$) and decreases

monotonously when ε_1 is increased from this value. This behaviour is consistent with Eq. (16), which predicts that $\text{Re } \omega_n/c$ is proportional to $1/\sqrt{\varepsilon_1 + 1}$. On the other hand, Figure 4b shows that $\text{Im } \omega_n/c$ are increasing functions of ε_1 , i.e., the multipolar plasmon damping rates ($|\text{Im } \omega_n|$) decrease as the value of the permittivity ε_1 increases. This behaviour, due to an increase in radiation losses when $\varepsilon_1 \rightarrow \varepsilon_2$, is not explained by Eq. (16).

To investigate the size dispersion of the localized plasmonic modes of graphene coated wires, in Figure ??(a) we plot the multipolar plasmon resonance frequency for $1 \leq n \leq 4$ modes as a function of R , remaining fixed parameters $\varepsilon_1 = 2.13$ and $\mu_c = 0.5$ eV. We can see that for R values between $0.1 \mu\text{m}$ and $4 \mu\text{m}$ the quasistatic limit given by equation (16) is a good approximation. For $R < 0.1 \mu\text{m}$, the interband term in equation (7), corresponding to the full retarded dispersion scheme, redshifts the resonances significantly. This same behaviour have been observed when the quasistatic limit approximation is applied to graphene coated dielectric spheres [?]. For large values of radius ($R > 0.4 \mu\text{m}$) the quasistatic limit blueshifts the resonances, an already observed feature in large bare particles [?]. In Figure 5(b) we illustrate the imaginary part of eigenfrequencies calculated with the FRD formulation (7) and the value of $\Im \omega_n/c = -\gamma/2$ calculated with the quasistatic approximation (16) (continuous line). We can see that the initial increase of the damping rates starting from the values $|\text{Im } \omega_n/c| \approx \gamma/2$ for given $1 \leq n \leq 4$ eigenmodes is followed by a decrease of $|\Im \omega_n/c|$ for sufficiently large particles. The initial increase of $|\Im \omega_n/c|$ with particle size, followed by the subsequent decrease for sufficiently large radius, as is illustrated in Figure 5(b), has been reported for the mode damping of silver and gold nanospheres [29].

B. Drude dispersive wires

In order to investigate the plasmonic features that a graphene coating can produce in intrinsically plasmonic wires, we consider graphene coated wires made of metallic-like substrates, that is, intrinsically plasmonic wires, where the localized surface plasmons of the graphene coating are expected to modify the localized plasmons already existing in the bare particle. We assume that the dispersive behavior of the interior electric permittivity is described by the Drude model given by equation (17). This model is applied to describe strongly doped semiconductors much larger in extent than the Fermi wavelength [4], which allow dynamic manipulation of carrier densities and

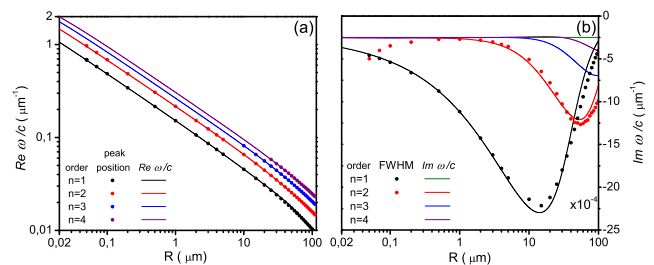


Fig. 5. $\text{Re } \omega_n$ (a) and $\text{Im } \omega_n$ (b), $n = 1, 2, 3$, and 4 , as functions of R . The parameters are $\mu_c = 0.5\text{eV}$, $\varepsilon_1 = 2.13$, $\gamma_c = 0.1$ meV, $\mu_1 = \mu_2 = 1$ and $\varepsilon_2 = 1$. Curves represent values obtained using Eq. (16), scatter symbols represent FR values. **Si les parece, se puede separar en dos paneles, uno arriba del otro, para que no quede tan apretada**

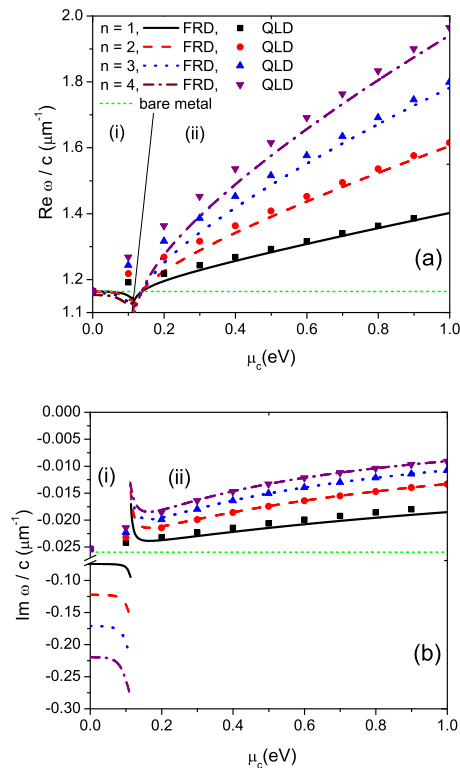


Fig. 6. Real (a) and imaginary (b) parts of the modal complex frequency for the n th mode ($1 \leq n \leq 4$) as functions of the chemical potential μ_c for a graphene coated metallic wire with radius $R = 50$ nm. The solid line curves corresponds to values calculated in the full retarded dispersion scheme (7) while the scatter symbols corresponds to values calculated by using the quasistatic approximation (equation (16)). The green dashed lines represents the values corresponding to the bare particle, for $n = 1, 2, 3,$ and 4 . The solid line in figure (a) separates two regions: region (i), where the interband transitions occur and region (ii), where only intraband transitions occur. $\epsilon_1(\omega)$ is given by equation (17), with $\epsilon_\infty = 3.72$, $\gamma_m = 0.01$ eV and $\hbar\omega_p = 0.5$ eV. Other parameters are $\gamma_c = 0.1$ meV, and $\mu_1 = \mu_2 = \epsilon_2 = 1$.

have plasma frequencies in the same range that the realizable Fermi energies of graphene. In Figures 6a and 6b we plot the curves corresponding to the plasmon resonance frequency and the corresponding damping rate, respectively, as a function of the chemical potential μ_c for $1 \leq n \leq 4$ eigenmodes. The interior electric permittivity $\epsilon_1(\omega)$ is given by equation (17) with $\epsilon_\infty = 3.72$ (corresponding to the residual high-frequency response of ZnO), $\gamma_m = 0.01$ eV and $\hbar\omega_p = 0.5$ eV. The multipolar plasmon eigenfrequencies ($1 \leq n \leq 4$) for the bare metallic cylinder are also given as a reference (green dotted line). Since the bare cylinder complex eigenfrequencies of the first four modes coincide in three significant figures, these modes are superimposed in Figures 6a and 6b. This behavior changes dramatically when the cylinder is wrapped with a layer of graphene, since as shown in the Figure 6a, the plasmon resonance frequencies of the modes are separated into more determined levels with increasing the chemical potential. For chemical potential values

where interband transitions occur (region i in Figure 6b), Figure 6b shows an increment of the multipolar damping rates with respect to the bare cylinder case. On the contrary, for μ_c values where only intraband transitions occur (region ii in Figure 6b), we see a decreasing of the damping rates with respect to the bare cylinder case. This behaviour, already noted in the recent work for spheres [?], is caused by the envelope of the graphene monolayer and can be used to reduce damping rates by varying the chemical potential μ_c . On the other hand, Figure ?? shows the corresponding multipolar eigenfrequencies curves (scatter curves) calculated by the quasistatic approach (21). As expected, we observe that this approach agree well with the values of complex frequencies calculated by using the full retarded dispersion scheme, in the whole range where only intraband transitions occur (region ii in Figure 6).

Falta comentar la figura que compara H vs NH y el caption.

5. CONCLUSION

In conclusion, we have presented a theoretical and numerical treatment to find the full characteristics of localized surface plasmons for circular cross-section wires coated with a graphene monolayer. The method can be regarded as an extension to the complex domain of the scattering formalism already used to evaluate the response of graphene-coated wires [?]. The method has been used to investigate how the size and dielectric permittivity of the wire substrate, as well as the chemical potential of the graphene monolayer, affects the complex eigenfrequencies of localized plasmonic modes supported by the wrapped graphene wire. We also compare resonant frequencies and damping rates calculated from this framework with those calculated from analytical expressions derived within of the quasistatic approximation. We presented examples for both dielectric (non-plasmonic) and like-metallic (plasmonic) wire substrates. In both cases, the examples show that the good tunability of the graphene coating leads to unprecedented control over the location and magnitude of the particle plasmonic resonances.

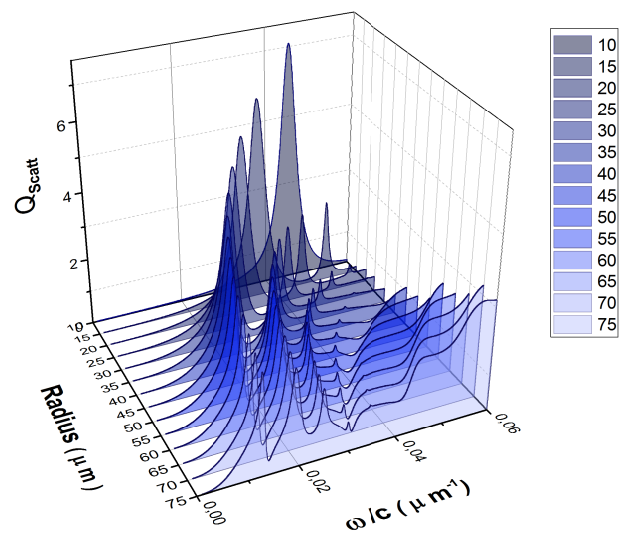


Fig. 7. Esta es la figura que compara H vs NH

ACKNOWLEDGMENT

The authors acknowledge the financial support of Consejo Nacional de Investigaciones Científicas y Técnicas, (CONICET, PIP 1800) and Universidad de Buenos Aires (project UBA 20020100100327).

6. FUNDING INFORMATION

Funding information should be listed in a separate block preceding any acknowledgments. List just the funding agencies and any associated grants or project numbers, as shown in the example below:

National Science Foundation (NSF) (1263236, 0968895, 1102301); The 863 Program (2013AA014402).

The acknowledgments may contain any information that is not related to funding:

The authors thank H. Haase, C. Wiede, and J. Gabler for technical support.

Do not use Funding Information or Acknowledgment headings.

7. REFERENCES

Note that *Optics Letters* uses an abbreviated reference style. Citations to journal articles should omit the article title and final page number. However, full references (to aid the editor and reviewers) must be included as well on a fifth informational page that will not count against page length.

REFERENCES

- M. Pelton and G. Bryant, Introduction to Metal-Nanoparticle Plasmonics, 1st ed. (Wiley, 2013).
- A. Brolo, "Plasmonics for future biosensors," *Nature Photonics* **6**, 709–713 (2014).
- Y. Fu, J. Zhang and J. Lakowicz, "Largely Enhanced Single-molecule Fluorescence in Plasmonic Nanogaps formed by Hybrid Silver Nanostructures," *Langmuir* **29**, 2731–2738 (2013).
- A. Schimpf, N. Thakkar, C. Gunthardt, D. Masiello and D. Gamelin, "Charge-Tunable Quantum Plasmons in Colloidal Semiconductor Nanocrystals," *ACS Nano* **8**, 1065–1072 (2014).
- P. West, S. Ishii, G. Naik, N. Emani, V. Shalaev, and A. Boltasseva, "Searching for better plasmonic materials," *Laser & Photon. Rev.* **4**, 795–808 (2010).
- A. Geim and K. Novoselov, "The rise of graphene," *Nature Mater* **6**, 183–191 (2007).
- M. Jablan, M. Soljacic, and H. Buljan, "Plasmons in Graphene: Fundamental Properties and Potential Applications," *Proceedings of the IEEE* **101**, 1689–1704 (2013).
- F. Rana, "Graphene terahertz plasmon oscillators," *IEEE Trans Nanotechnol.* **7**, 91–99 (2008).
- M. Jablan, H. Buljan, and M. Soljacic, "Plasmonics in graphene at infrared frequencies," *Phys. Rev. B* **80** (24), 245435 (2009).
- A. Y. Nikitin, F. Guinea, F. J. García-Vidal, and L. Martín-Moreno, "Edge and waveguide terahertz surface plasmon modes in graphene microribbons," *Phys. Rev. B* **84**, 161407 (2011).
- J. Christensen, A. Manjavacas, S. Thongrattanasiri, F. H. Koppens, and F. L. García de Abajo, "Graphene plasmon waveguiding and hybridization in individual and paired nanoribbons," *ACS Nano* **6** (1), 431–440 (2012).
- P. Liu, X. Zhang, Z. Ma, W. Cai, L. Wang, and J. Xu, "Surface plasmon modes in graphene wedge and groove waveguides," *Opt. Express* **21** (26), 32432–32440 (2013).
- X. He, Z. Liu, D. Wang, M. Yang, T. Hu and J. Tian, "Saturable absorber based on graphene-covered microfiber," *IEEE Photon. Technol. Lett.* **25**, 1392–1394 (2013).
- X. He, X. Zhang and M. Xu, "Graphene covered on microfiber exhibiting polarization and polarization-dependent saturable absorption," *IEEE J. Sel. Top. Quantum Electron.* **20**, 4500107 (2014).
- Y. Wu, B. Yao, A. Zhang, Y. Rao, Z. Wang, Y. Cheng, Y. Gong, W. Zhang, Y. Chen, and K. S. Chiang, "Graphene-coated microfiber Bragg grating for high-sensitivity gas sensing," *Opt. Lett.* **39** (5), 1235–1237 (2014).
- W. Li, B. Chen, C. Meng, W. Fang, Y. Xiao, X. Li, Z. Hu, Y. Xu, L. Tong, H. Wang, W. Liu, J. Bao, and Y. R. Shen, "Ultrafast all-optical graphene modulator," *Nano Lett.* **14**, 955–959 (2014).
- J. W. Ko, S.-W. Kim, J. Hong, K. Kang, and C. B. Park, "Synthesis of graphene-wrapped CuO hybrid materials by CO₂ mineralization," *Green Chem.* **14** (9), 2391–2394 (2012).
- J. S. Lee, K. H. You, and C. B. Park, "Highly photoactive, low bandgap TiO₂ nanoparticles wrapped by graphene," *Adv. Mater.* **24** (8), 1084–1088 (2012).
- J. S. Lee, S. I. Kim, J. C. Yoon, and J. H. Jang, "Chemical Vapor Deposition of Mesoporous Graphene Nanoballs for Supercapacitor," *ACS Nano* **7**, 6047 (2013).
- H. Yang, Z. Hou, N. Zhou, B. He, J. Cao, and Y. Kuang, "Graphene-encapsulated SnO₂ hollow spheres as high-performance anode materials for lithium ion batteries," *Ceramics International* **40**, 13903 (2014).
- B. Zhu, G. Ren, Y. Gao, Y. Yang, Y. Lian, and S. Jian, "Graphene-coated tapered nanowire infrared probe: a comparison with metal-coated probes," *Opt. Express* **22**, 24096 (2014).
- Y. Gao, G. Ren, B. Zhu, H. Liu, Y. Lian, and S. Jian, "Analytical model for plasmon modes in graphene-coated nanowire," *Opt. Express* **22**, 24322 (2014).
- Y. Gao, G. Ren, B. Zhu, J. Wang, and S. Jian, "Single-mode graphene-coated nanowire plasmonic waveguide," *Opt. Lett.* **39**, 5909 (2014).
- T. Christensen, A. P. Jauho, M. Wubs, and N. Mortensen, "Localized plasmons in graphene-coated nanospheres," *Phys. Rev. B* **91**, 125414 (2015).
- M. Farhat, C. Rockstuhl, and H. Bağcı, "A 3D tunable and multi-frequency graphene plasmonic cloak," *Opt. Express* **21**, 12592 (2013).
- R. J. Li, X. Lin, S. S. Lin, X. Liu, and H. S. Chen, "Tunable deep-subwavelength superscattering using graphene monolayers," *Opt. Lett.* **40**, (2015).
- M. Riso, M. Cuevas, and R. A. Depine, "Tunable plasmonic enhancement of light scattering and absorption in graphene-coated subwavelength wires," *Journal of Optics* **17**, 075001 (2015).
- O. J. F. Martin, "Plasmon resonances in nanowires with nonregular cross-section," in *Optical Nanotechnologies: The Manipulation of Surface and Local Plasmons*, J. Tominaga, and D. P. Tsai (Eds.), *Topics Appl. Phys.* **88**, 183–210 (Springer-Verlag, 2003).
- K. Kolwas, and A. Derkachova, "Damping rates of surface plasmons for particles of size from nano- to micrometers; reduction of the non radiative decay," *Journal of Quantitative Spectroscopy & Radiative Transfer* **114**, 45–55 (2003).
- L. A. Falkovsky, "Optical properties of graphene and IV–VI semiconductors," *Physics Uspekhi* **51**, 887–897 (2008).
- S. A. Milkhailov, K. Siegler, "New Electromagnetic Mode in Graphene," *Physical Review Letters* **99**, 016803 (2007).
- M. Abramowitz, and I. A. Stegun (Eds.), *Handbook of Mathematical Functions with Formulas, Graphs, and Mathematical Tables*, 10th ed. (Dover, 1972).
- I. Novotny, and B. Hecht, *Principles of Nano-Optics*, 1st ed. (Cambridge Press, 2006).
- Z. R. Huang, L. L. Wang, B. Sun, M. D. He, J. Q. Liu, H. J. Li, and X. Zhai, "A mid-infrared fast-tunable graphene ring resonator based on guided-plasmonic wave resonance on a curved graphene surface," *J. Opt.* **16**, 105004 (2014).